Silica-induced electron loss of silver nanoparticles

Magali Benoit, Joël Puibasset, Caroline Bonafos, Nathalie Tarrat

Journal Name

ARTICLE TYPE

Cite this: DOI: 00.0000/xxxxxxxxxx

Silica-induced electron loss of silver nanoparticles

Magali Benoit*[a], Joël Puibasset[b], Caroline Bonafos[a] and Nathalie Tarrat*[a]

Received Date
Accepted Date

DOI: 00.0000/xxxxxxxxxx

Despite the frequent use of silver nanoparticles (Ag NP) embedded in materials for medical or optical applications, the effect of the matrix on the nanoparticles properties remains largely unknown. This study aims to shed light on the effect of an amorphous silica matrix on the structure and charge distribution of 55- and 147-atoms silver nanoparticles by means of dispersion-corrected DFT calculations. Particular attention is paid on nanoparticle size and concentration effects and on the impact of the presence of native defects in the matrix. Covalent bonding between the silver nanoparticles and the matrix are found to occur at the interface. Such interface reconstruction involves the breaking of Si-O bonds, which systematically leads to the formation of Ag-Si bonds, and in some cases, to the formation of Ag-O ones. Interestingly, these interface reconstructions are accompanied by an electron depletion of the nanoparticle, a substantial number of electrons being transferred from the two outer shells of the Ag NP towards the surrounding silica medium. The electrons lost by the nanoparticle are captured by the Si atoms involved in the interface bonds, but also, unexpectedly, by the undercoordinated silica defects that act as electron pumps and by the atoms of the silica network inside a spherical shell of a few angströms around the silver nanoparticle. The number of interface bonds and of electrons transferred to the surrounding silica shell appears to be proportional to the surface area of the Ag NP. The electronic extension within the silica goes beyond that attributable to the Ag NP spill-out. The presence of additional electrons in the matrix, especially on defects, is consistent with the experimental literature.

1 Introduction

Silver nanoparticles (Ag NPs), extensively studied in recent years due to their remarkable biological[1] and optical properties[2], find many applications in sensing[3–5], optoelectronics[6] and as antimicrobials[7–9]. However, because of their toxicity[10,11] and their high propensity for oxidation[12] and sulfidation[13,14], these nanoparticles require to be incorporated into a matrix for many applications[15]. For instance, incorporating Ag NPs into polymers used as base materials for many medical devices has made it possible to prevent bacterial growth *via* silver ions release while protecting people in contact with these nanocomposites from the Ag NPs toxicity[16–19]. In the case of devices that take advantage of the remarkable optical properties of the Ag NPs, their embedding in matrices prevents their agglomeration and allows to stabilize and organize them in space, but also to tune their properties. Indeed, the underlying physical phenomenon at the origin of the Ag NPs optical properties, called localized surface plasmon resonance (LSPR, a collective oscillation of the conduction electrons in response to a shift from their equilibrium position induced by the interaction of the nanoparticle with light), depends on the size of the particles, their shape, their density and spatial arrangement, but also on the properties of the surrounding medium[20–22]. When an Ag NP is embedded, the coherent electron oscillation induces a polarization of the matrix which in response shifts the LSPR in a matrix-dependent way[2,23]. For instance, the surface plasmon resonance of Ag NPs embedded in silica can be tuned by adjusting the silica thickness around the nanoparticles[24–26]. Moreover, the presence of adsorbates in the vicinity of the Ag NPs surfaces induces local refractive index modifications of the surrounding medium, leading to a shift of the LSPR. This latter can be monitored, allowing the use of such devices as sensors[27–29]. However, although it is clearly established that the environment strongly influences the electronic properties of the Ag NPs, the phenomena at play at the atomic scale and the precise effect of the matrix on the physical properties of these particles remains poorly known.

Regarding the effect of the presence of amorphous silica around the nanoparticles, the impact of the matrix on the atomic structure of embedded Ag NPs depends on the nanoparticle size. Indeed, for small clusters, the encapsulation in SiO_2 leads to a modi-

[a] *CEMES, CNRS and Université de Toulouse, 29 rue Jeanne Marvig, 31055 Toulouse, France. E-mail: magali.benoit@cemes.fr, nathalie.tarrat@cemes.fr*
[b] ICMN - Université d'Orléans, CNRS, 1b rue de la Férollerie, CS 40059, 45071 Orléans Cedex 2, France

fication of the Ag-Ag bond lengths within the cluster[30]. For larger nanoparticles, a high-resolution electron microscopy study[31], focused on the effect of a surrounding silicate glass matrix on the shape and internal structure of Ag NPs, concluded that the embedded forms are comparable to those supported on oxides. The relative stability of these latter was reported to be significantly different from those observed in vacuum. Indeed, a molecular simulation study has shown that the hierarchy of equilibrium morphology is affected by the presence of the substrate[32]. The aging of embedded nanoparticles has also been studied, mainly due to their tendency to oxidation. By observing the disappearance of the plasmonic resonance of Ag NPs embedded in silica on time scales ranging from a few days to a few weeks, Hillenkamp *et al.* concluded that nanometric silver clusters are unstable at ambient conditions due to gradual oxidation whatever the preparation conditions[33]. This conclusion is strongly questioned by a study of Benzo *et al.* on a time scale of months which shows that much less mesoporous samples synthesized by ultra-low energy ion implantation and annealed at intermediate temperature under N_2 remain stable.[34].

The way the surrounding environment affects the properties of Ag NPs is most likely related to the nature of the interface between these nanoparticles and the matrix in which they are embedded. In the literature, the interface between an Ag NP and a silica matrix has been described as moderate to strong, some studies having even evidenced the covalent nature of some interactions. In a Density Functional Theory (DFT) study conducted on quartz[35], short interfacial distances (between 1.7 and 2.4 Å) and strong work of adhesion (between 2.67 and 7.86 J/m^2) have been reported, both depending on the type of atoms terminating the silica surface and on the interface configuration. Short interface bonds (around 2.1 Å) have also been reported between non-bridging oxygen centers on a crystalline SiO_2 surface and small silver clusters[36]. In the case of amorphous silica, a redshift in the Fourier Transformed Infra-Red (FTIR) spectrum of Ag NPs (with an average diameter of 12 nm) dispersed in a silica matrix has been interpreted by the formation of Si–O–Ag bond[37,38]. The covalent nature of such interface bonds has been confirmed by Balout *et al.*, who have reported spontaneous breaking of the interfacial Si–O bonds and formation of covalent O–Ag and Si–Ag bonds by performing DFT calculations on model systems of the interfaces between amorphous silica and three silver crystalline facets[39]. In this study, the work of adhesion has been found much lower than the ones reported by She *et al.*[35], with values ranging between 0.3 and 0.6 J/m^2. Note that the appearance of a new Raman mode in the case of silver nanocluster embedded in amorphous silica had been reported twenty years ago by Gangopadhyay *et al.* but at that time it was interpreted as corresponding to dispersed Ag atoms bonded with the interstitial-oxygen defect caused by irradiation and not to interface bonds[40].

Although it is known that electron transfer properties of Ag NPs depend on their shape and size[41,42], the charge transfers taking place at the interface between Ag NPs and silica have scarcely been discussed in the literature. Charge transfer between metals and insulating oxides are often considered to be very local and confined to the interfaces. However, for multilayer models such as metal/SiO_2/Si, electron have been reported to tunnel through the thin oxide layers, allowing long-range charge transfer[43]. By investigating the interaction between SiO_2 thin films and silver particles via X-ray photoelectron spectroscopy experiments, Komiyama *et al.* have observed a partial reduction of Si(IV) atoms[44], concluding on this basis that the Ag NPs deposited on silica are positively charged[45]. This experimental observation is in line with the theoretical study of Ferullo *et al.* which report an electronic charge transfer from the metal particle to the support for silver clusters of extremely small size (up to 3 atoms) deposited on a defective SiO_2 surface[46]. Although a deep knowledge of the charge state of Ag NPs is very important for many applications such as plasmonics[47,48], the effect of the surrounding matrix on the particle charge has never been quantified, to the best of our knowledge.

The main objective of the present study is to fill this gap by investigating the electronic properties of Ag NPs embedded in silica by means of DFT calculations. The paper is organized as follows. After a brief description of the investigated systems, the structural and electronic properties of a 147-atom Ag NP embedded in a silica matrix are thoroughly analyzed. Covalent bonding between the Ag NP and the matrix are found at the interface and charge transfers take place from the Ag NP towards the surrounding medium. The effects of the native defects in the matrix, of the size of the nanoparticle as well as of the distance between embedded nanoparticles are subsequently investigated and the results are compared with the literature. In a final part, we draw a conclusion followed by a thorough discussion of the implications of our results for experiments, in particular with regard to conductivity of Ag-SiO_2 nanocomposites as well as chemical, electrochemical and optical properties of embedded Ag NPs.

2 Methodology

2.1 Preparation of the systems

The system considered is a Ag NP embedded in a silica SiO_2 matrix inside a cubic box with periodic boundary conditions (PBC). The statistical ensemble is chosen to be isothermal-isochoric with a fixed number of atoms. The temperature is denoted T and the simulation box size L. The number of Ag atoms is imposed by the nanoparticle size and structure. Ag NPs with 2 different symmetries have been considered (icosahedron and cuboctahedron) in silica: DFT relaxation always leads to the icosahedral structure (Ih) (see Figure S1 of the Supp. Info). We thus consider two Ih structures with 55 and 147 atoms.

The number of silica species in the box is chosen so that the density of the silica matrix surrounding the nanoparticle is as close as possible to the experimental value for amorphous silica (≈ 2.2 g/cm^3). Note that the silica density being inhomogeneous in the vicinity of the NP, a reliable value is obtained by measuring the density out of a sphere centered on the Ag NP and of radius 4 Å larger than the Ag NP.

The first system is an icosahedral 147-atoms Ag NP embedded in 390 SiO_2 in a cubic box of size $L = 27.6$ Å with PBC (called hereafter L-Ag_{147} or L*-Ag_{147}, if the silica matrix contains defects). In order to investigate Ag NP size effects, a second system is built

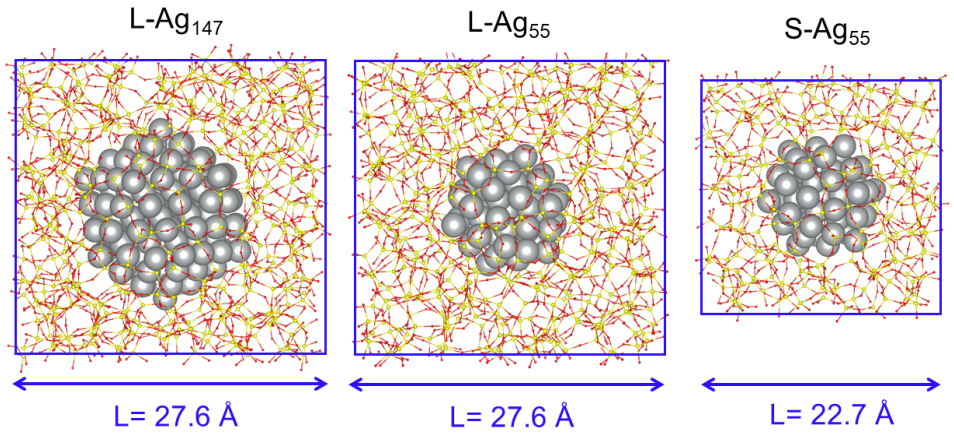

Fig. 1 Snapshots of the Ag NP in amorphous SiO_2 after DFT relaxation. Left: Ag_{147} and 390 SiO_2 in a cubic box of edge length L=27.6 Å(L-Ag_{147}). Center: Ag_{55} and 430 SiO_2 in a cubic box of L=27.6 Å(L-Ag_{55}). Right: Ag_{55} and 230 SiO_2 in a cubic box of L=22.7 Å(S-Ag_{55}). Ag atoms: grey balls; Si and O atoms: yellow and red sticks, respectively.

with an icosahedral 55-atom Ag NP surrounded by 430 SiO_2 in a box of the same size $L = 27.6$ Å (called hereafter L-Ag_{55}). Note that this configuration leads to a thicker silica wall between the periodic images of the Ag NP. Therefore, to investigate the effects of the interactions between Ag NPs embedded in SiO_2, we considered a third system with 55 Ag atoms, 230 SiO_2 and $L = 22.7$ Å (called hereafter S-Ag_{55}) so that the silica walls are of comparable size with those of the L-Ag_{147} system. The principal characteristics of the investigated models are summarized in Table 1 and the corresponding atomic models are depicted in Figure 1. The preparation of the systems by means of Monte Carlo equilibration and the subsequent DFT relaxations are described hereafter.

Table 1 Number of Ag atoms (N_{Ag}) and SiO_2 units (N_{SiO_2}), cubic box edge length (L), smallest silica wall thickness between the Ag NP and its periodic images (L_w) and number of defects in the silica matrix ($N_{defects}$) in the four investigated systems.

Systems	N_{Ag}	N_{SiO_2}	L [Å]	L_w [Å]	$N_{defects}$
L-Ag_{147}	147	390	27.6	≈13.7	0
L*-Ag_{147}	147	390	27.6	≈13.7	4[a]
L-Ag_{55}	55	430	27.6	≈18.5	0
S-Ag_{55}	55	230	22.7	≈13.5	0

a. 1 Non-bridging oxygen atom (NBO), 1 SiO_3, 1 SiO_5, 1 OSi_3

2.2 Monte Carlo equilibration of the silica matrix

The systems are prepared as follows. The stable NP structure obtained after DFT equilibration in vacuum is positioned at the center of the simulation box with the silica species randomly distributed in the empty space around. A Monte Carlo (MC) run is performed at high temperature (5000 K) with empirical potentials for silica species and silver-silica interactions. Note that the Ag atoms are frozen during the course of the simulation to preserve the NP's structure. The potential used for silica (TTAMm)[49,50] has proven to be an efficient pairwise potential to reproduce its structures, including the amorphous phase. The Ag-SiO_2 interaction is described with a simple van der Waals like potential that reproduces wetting angle measurements for Ag NP deposited on silica glass or oxidized Si wafers[51?]. After thermal equilibration, the temperature is slowly decreased in order to produce a stable structure. As long as the temperature lies above 2500 K, the system equilibrates quite rapidly ($> 10^6$ MC steps/atom). However, below this value, the relaxation times become rapidly out of reach for molecular simulations, and the system remains trapped around a local minimum associated with an amorphous structure. This structure is made of randomly associated SiO_4 tetrahedra, with isolated defects such as Si-O dangling bonds with a non-bridging oxygen atom (NBO), under- or over-coordinated Si (SiO_3 or SiO_5) or tricluster oxygens (OSi_3). Despite the fact that the molecular simulation time scale is quite short, the obtained structures are believed to be realistic, in particular regarding the presence of defects. We have thus monitored the number of defects during the quench procedure, in order to select configurations with or without defects. For all systems, defect-free configurations have been selected. In order to evaluate the effect of defects, we have selected a configuration with four defects (1 NBO, 1 OSi_3, 1 SiO_3 and 1 SiO_5) for the L-Ag_{147} system, named hereafter L*-Ag_{147}.

The structure of amorphous silica around the Ag clusters has been assessed by computing the pair correlation functions g(r), the angular distributions and the rings statistics (Figure S2 of Supp. Info).

2.3 DFT calculations

Once the systems are equilibrated at 300 K using the empirical potentials, selected configurations are taken as initial positions for DFT relaxations of the atomic positions. DFT calculations were carried out using the VASP package with PAW pseudopotentials for Ag, Si and O. The PBE exchange and correlation functional[52] was used with dispersion corrections of the Grimme D3 type[53]. The choice of this functional was dictated by the good results obtained on the Ag/SiO_2 interfaces[39]. In a first step, the wavefunctions were expanded in plane waves at the Γ-point up to an energy cutoff of 300 eV for fast relaxations, then the cutoff was increased to 500 eV for more accurate calculations. A Gaussian

smearing was applied with a parameter of 0.05 eV. The atomic positions were relaxed until atomic forces reached 0.01 eV/Å ^{2}. The evolution of the total energy of the system during the successive relaxation steps and the corresponding structures are shown in the Supp. Info (Figures S3, S4 and S5).

3 Results

3.1 Ag_{147} in SiO_2

Figure 2 presents the structure of L-Ag_{147} system after relaxation. At the interface between the Ag NP and the silica matrix, we observe three spontaneous reconstructions consisting in the breaking of Si-O bonds and the formation of bonds between these silica atoms and Ag atoms of the nanoparticle surface. The silica rings that open during these reconstructions and the silica atoms that bind to the Ag NP are magnified in Fig. 2 (labels **1**, **2** and **3**), and the associated modifications of the electronic density are depicted in Fig. 2(b) and magnified in Fig (d). Such interface reconstruction has already been observed in planar interfaces between Ag(100), Ag(110) and Ag(111) surfaces and amorphous silica[39].

In one case (label **1** in Figure 2(a) and (c)), the Si-O bond breaks and the Si and O atoms of this bond (herafter denoted Si* and O*) bind to two Ag atoms of the NP surface. As it can be seen in Figure 2(c), the broken Si-O bond belongs to a 5-membered ring perpendicular to the NP surface. The O* atom remains linked to only one Si atom with a short bond of 1.58 Å (see Figure 2(c)). Most of the electronic charge is then transferred to the Si* atom which carries a charge of 2.21e, the O* atom having a charge of -1.44e. These values should be compared to the average charges of Si and O in bulk amorphous SiO_2 (3.2e and -1.6e, respectively). The Si*-Ag and O*-Ag bond distances are of 2.42 Å and 2.26 Å and some charge is also transferred to the Ag atoms (leading to charges of -0.09e when bonded to Si and +0.20e when bonded to O). The Si*-Ag and O*-Ag bond distances are close to those found in our previous works on the Ag/SiO_2 planar interfaces[39], on Ag_2O bond lengths[54] and to the typical Ag-O bond lengths found in small Ag_n-O_2 clusters[55] which range between 2.2 and 2.6 Å.

In Figure 2(b) and 2(d), the electronic density difference is shown as isosurfaces at +0.003e/Å^3 (green) and -0.003e/Å^3 (blue): it is obtained by subtracting to the electronic density of the system, that of the Ag NP alone and that of the SiO_2 matrix alone. In the region where the Si-O bonds have broken and new bonds with Ag have formed (Figure 2(d), label **1**), we notice a significant electron density reorganization, especially between the Ag atoms and the Si* and O* ones, suggesting the formation of covalent bonds.

In the case of labels **2** and **3** (Figure 2(a) and (c)), when the Si-O bond breaks, only the Si* atom binds to one Ag atom of the NP surface, the O* atom going away from the NP surface and becoming a NBO instead of forming a O-Ag bond. This can be explained by the fact that, in these two last cases, the broken Si-O bond belongs to a 4-membered ring parallel to the NP surface, whereas in the first case, the Si-O bond belongs to a 5-membered ring perpendicular to the surface. One can then assume that the strain on the bonds of the 4-membered ring are at the origin of the displacements of the O* atom away from the NP surface. As for the first case, the remaining O*-Si bonds are short (1.55 Å in both cases). The charges carried by the Si* atoms are of 2.22e and 2.19e and the one carried by the corresponding O* atoms are of -1.47e and -1.51e. We observe in both cases the formation of Si*-Ag bonds whose lengths are 2.51 Å and 2.58 Å , with a charge of -0.08e and of -0.02e on the corresponding Ag atoms. As for label **1** , the electronic density differences are shown in Figure 2(d) with magnifications of the reconstructed interfaces (labels **2** and **3**). One can see again some electronic density between the Si and Ag atoms, indicating the formation of Si*-Ag bonds. Important redistribution of the electronic density is also visible at the O* sites.

Apart from these interface bonds, we also observe a modification of the electronic density in many other places in silica, *i.e.* not only at the three interface reconstruction locations, but also away from these areas as can be seen, for instance, on the right side of the nanoparticle in Figure 2(b). This result indicates that the presence of the Ag NP inside the silica matrix affects this latter beyond the sole formation of the bonds at the interface.

Moreover, these interface reconstructions are also accompanied by a significant reorganization of the charges in the Ag NP (Figure 3(a), second column) compared with those of the same Ag NP in vacuum (Figure 3(a), first column). Positive charges are indicated in blue and negative ones in red. In vacuum, the surface atoms are negatively charged with the largest charges on the vertex atoms. When the Ag_{147} NP is embedded in the SiO_2 matrix, the charge distribution at the NP surface is very different: The vertex atoms are no longer negatively charged and the Ag atoms bonded to the Si* and O* atoms become negatively and positively charged, respectively. Moreover, the whole Ag NP surface appears to be rather positively charged. Inside the Ag NP, we do not observe significant modifications of the charges, except for the central atom.

This new distribution of the charges inside the Ag_{147} NP is accompanied by a modification of its structure, in particular at the surface and subsurface. In Figure 3(b), the charge on each Ag atom of the NP is shown as a function of its distance from the center of the NP. The positions and charges of the Ag_{147} NP in vacuum are depicted by red circles: each layer of the icosahedron is well defined and one can clearly see the vertex atoms at a distance of $\approx$ 8.4 Å which carry a charge of $\approx$ -0.07e. Once the Ag_{147} NP is embedded in the SiO_2 matrix, the distribution of charges is strongly modified and the distances show a significant alteration (empty blue squares in Figure 3(b)). Most of the surface and subsurface Ag atoms become positively charged and the positions of the atoms of the outermost layers are slightly modified. The center of the NP is also impacted, the charge of the center atom changing from almost 0 to -0.05e. Finally three of the Ag atoms that are bonded to Si* and O* atoms are easily identified, as the two empty blue squares at a distance of 7.4 Å and 7.8 Å with a charge of $\approx$ -0.08e and -0.09e (for Si*-Ag) and the empty blue square at a distance of 7.0 Å and a charge of $\approx$ +0.2e (for O*-Ag), respectively. The charge on the 4th Ag atom involved in a Si*-Ag bond changes by only -0.02e.

As a consequence, the Ag_{147} NP embedded in SiO_2 becomes

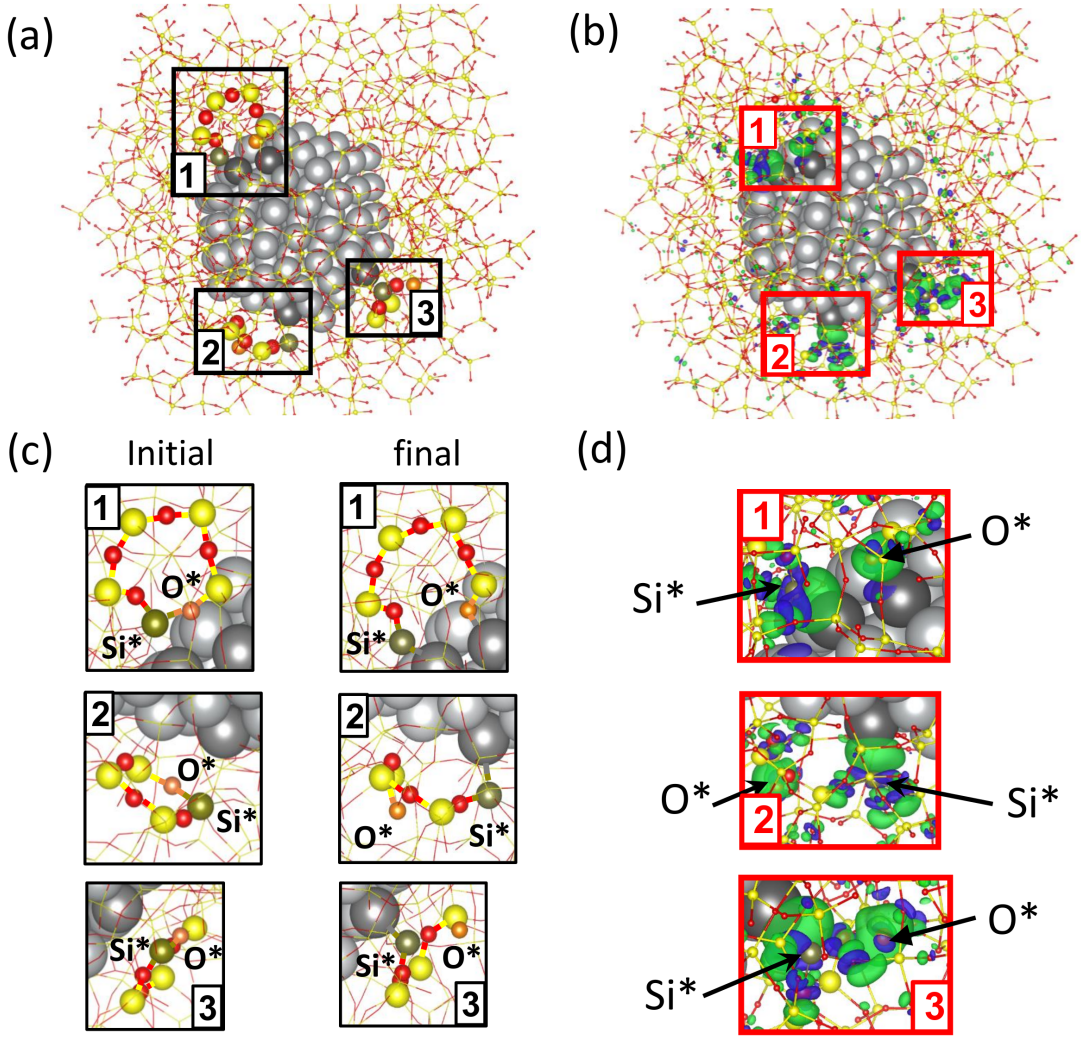

Fig. 2 a) L-Ag_{147} after relaxation (Ag in grey, O in red and Si in yellow). The silica atoms represented by balls are those belonging to the rings that have opened. The balls in brown and orange are the Si and O atoms of the broken bonds, respectively, and the balls in dark grey are the Ag atoms that bind to the Si or O atoms. b) Isosurface of the electronic density difference (see text): +0.003 $e/Å^3$ (green), -0.003 $e/Å^3$ (blue). Magnifications, labels **1**, **2** and **3**, of the broken rings before and after relaxation (c) and of the isosurfaces around the broken rings (d). Si^* and O^* denote the atoms belonging to the broken bonds.

positively charged with a total charge of +4.35e. We have seen that some of these electrons are uptaken by the Si^* atoms bound to the Ag surface atoms. However, these electronic transfers are not sufficient to quantitatively explain the electron depletion of the Ag NP. In order to determine where these electrons went, we performed DFT relaxation on the same system where the Ag NP has been removed, leading to a cavity in silica. (Note that the cavity was created in the configuration obtained after Monte Carlo relaxation of the silica around the Ag NP, prior to the DFT runs). The charges carried by the Si and O atoms after DFT relaxation in the silica + Ag NP system are then compared to those carried by the same atoms after DFT relaxation in the silica + cavity system. In doing so, we can determine which atoms have captured most of the electrons from the Ag NP.

Firstly, the Si^* atoms of the 3 broken Si-O bonds gained -0.92e, -0.95e and -0.93e with the Ag NP with respect to their charge with the cavity. The corresponding O^* atoms' charges remain unchanged except for the one that binds to a Ag surface atom, whose charge is less negative by +0.22e. This makes a balance of -2.58e on these atoms which does not compensate the loss of +4.35e by the Ag NP (see Table 2). The remaining electronic density is thus delocalized over the atoms in the matrix but mainly on the O atoms. Indeed, once the charge differences on the remarkable Si^* atoms are removed, the remaining charge difference on the Si atoms between the systems with and without the Ag NP is of -0.19e. Conversely, the remaining charge difference on the O atoms (without that corresponding to the remarkable O^* atoms) is equal to -1.58e. In summary, the 4.35 electrons lost by the Ag_{147} NP go mostly to the Si^* and O^* atoms bound to the nanoparticle, but a non-negligible amount (about 40%) is distributed over the rest of the silica matrix, mainly on the oxygen atoms.

The charge differences on the atoms of the silica matrix with and without the Ag NP, has been monitored as a function of the distance to the center of the Ag NP (Figure 4). We observe that

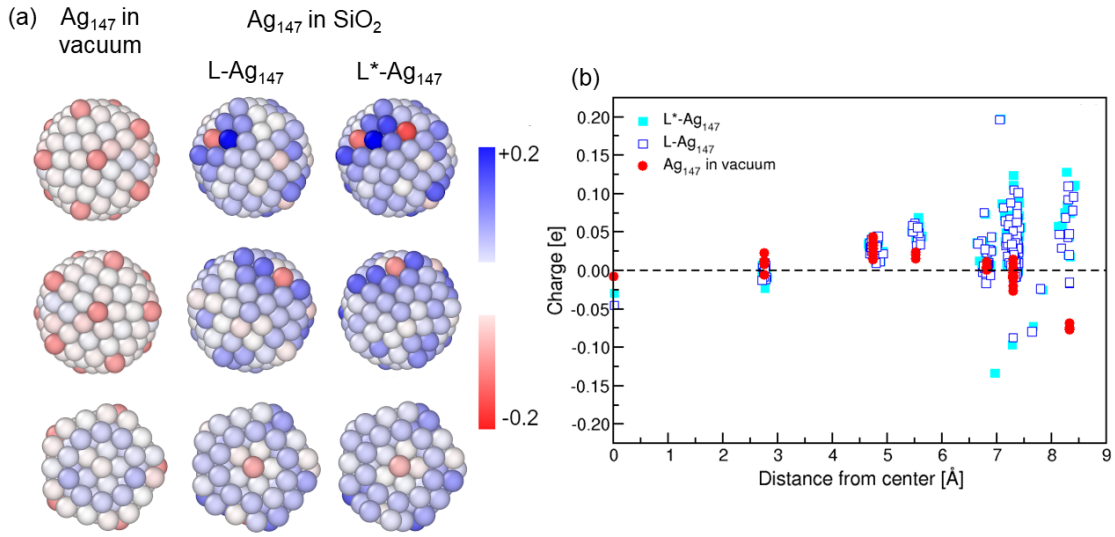

Fig. 3 (a) Charges on the Ag atoms of the Ag_{147} NP in vacuum (left), in the SiO_2 matrix without defects (L-Ag_{147}, center) and in the SiO_2 matrix with defects (L*-Ag_{147}, right).(b) Evolution of the atomic charges on the Ag atoms as a function of their distance to the center of the mass of the NP: Ag_{147} in vacuum (red circles), embedded in SiO_2 L-Ag_{147} (empty blue squares) and embedded in SiO_2 with defects L*-Ag_{147} (full cyan squares).

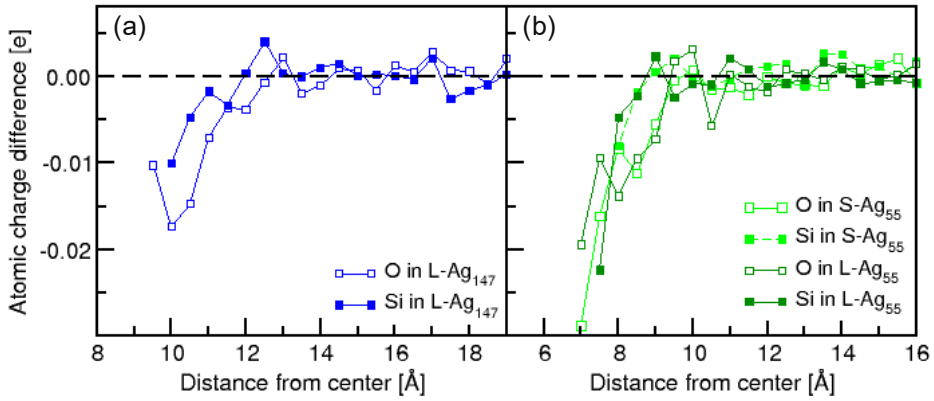

Fig. 4 Charge difference per atom on the O and Si atoms inside the SiO_2 matrix with and without Ag NP, as a function of their distance from the NP center: (a) L-Ag_{147}; (b) L-Ag_{55} and S-Ag_{55}. The differences were averaged over atoms inside spherical layers of 0.5 Å width.

Table 2 Charge distribution in the different systems. q_{AgNP} is the total charge on the Ag NP. Δq_X is the total charge difference on the X species between the systems with and without the Ag NP: X = Si*(O*) for the silica species involved in broken bonds; X = Si(O) for the silica species not involved in broken bonds; X = defects for the 4 defects of L*-Ag147. The total charge differences (except that of the defects) sum up to zero.

	q_{AgNP}	Δq_{Si^*}	Δq_{O^*}	Δq_{Si}	Δq_{O}	$\Delta q_{defects}$
L-Ag_{147}	+4.35	-2.80	+0.22	-0.19	-1.58	
L*-Ag_{147}	+5.05	-2.75	+0.24	-0.87	-1.67	-0.95
L-Ag_{55}	+2.53	-1.80	+0.29	-0.10	-0.92	
S-Ag_{55}	+1.82	-0.93	+0.12	+0.06	-1.07	

the additional electrons on the O atoms extend on a spherical shell of ≈ 4 Å from the silica inner surface within the matrix. We also tried to analyse whether the charge variations on the Ag atoms in the NP were correlated to their distance from the closest Si and O atoms in the silica (see Figure S6 of Supp. Info). No conclusive statement could be made for Ag atoms in the core of the NP. However, for Ag atoms at the interface, a correlation can be pointed out between the charge and the distance to the nearest silica species, without clear difference between O and Si. The behavior of the Ag atoms involved in bonding clearly departs from the others in sign and magnitude.

3.2 Influence of SiO_2 native defects on the electronic properties

As presented in the Methodology section, we have also prepared a system in which the Ag_{147} NP has been embedded in the same silica matrix but containing several defects, namely one SiO_5, one SiO_3, one OSi_3 and one NBO. For optimizing the atomic positions, the same protocol than the one used for the L-Ag_{147} model has been applied. The evolution of the total energy of the system during the successive relaxation steps and the corresponding structures are shown in the Supp. Info (Figure S4). Note that

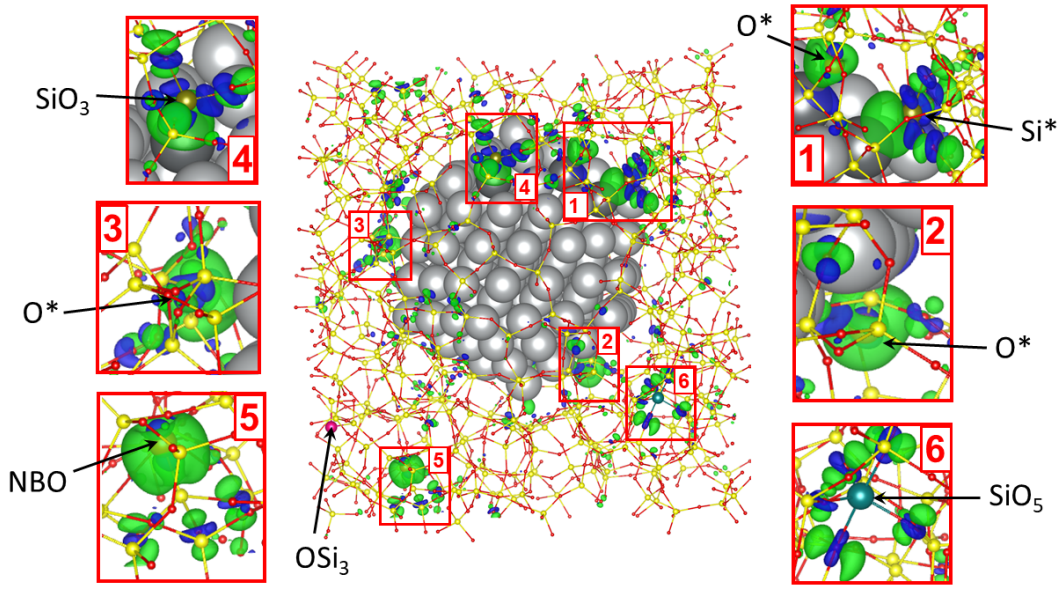

Fig. 5 Isosurface of the electronic density difference for L*-Ag_{147} NP after relaxation. Positive values are shown in green, negative values in blue. The insets show magnifications of the defects in the silica matrix and bonding to the Ag NP.

since the silica matrix is the same for both systems except for the defects present in L*-Ag_{147}, the breaking of the same Si-O bonds as well as the formation of the same bonds with the Ag surface atoms occur than in the L-Ag_{147} system. This makes possible the analysis of the effect of a defective matrix, all things being otherwise equal. The only noticeable difference at the interface comes from the formation of an additional bond between the Si of the SiO_3 defect, which is close the Ag NP surface, and a Ag surface atom.

Figure 5 shows the isosurfaces of the electronic density difference between that of the L*-Ag_{147} NP and that of the two isolated subsystems. As in the case of the non-defective silica matrix, significant changes in electron density are observed at the interface where the reconstructions took place and where the Si*-Ag and O*-Ag bonds are formed. (Note that the point of view being different in Figure 5 and in Figure 2(b), some of the Si*-Ag bonds cannot be seen). However, surprisingly, green isosurfaces can also be observed at other locations in the silica matrix far from the interface, notably on the NBO and on the SiO_5 defects (insets **5** and **6** in Figure 5). These isosurfaces indicate that these defects have gained some electronic density due to the presence of the Ag_{147} NP, even though they are not directly in contact with it. As a consequence, the Ag_{147} NP looses more electrons when embedded in a defective silica matrix and carries a charge of $+5.05e$. The variation of the charge distribution is depicted in Figure 3(a) (right column) and in Figure 3(b) (cyan squares). Compared to the L-Ag_{147} system, we observe in Figure 3(a) an additional negatively charged Ag surface atom which is due to the creation of a Si*-Ag bond with the SiO_3 defect. The charge of this Ag atom is around -0.13e as evidenced in Figure 3(b) (cyan square around 7 Å from the NP center).

By following the same protocol as for the non-defective silica, *i.e.* by comparing the charges on the whole system to those of the defective SiO_2 matrix with an empty cavity in place of the Ag NP, it is possible to determine which atoms of the silica matrix have seen their charge changed. First, the Si* atoms carry charges of $+2.23e$, $+2.23e$, $+2.20e$ which makes a total charge difference of -2.75e on these atoms in the system with the Ag NP compared to that with the cavity (see Table 2). Regarding the oxygen atoms, the O* atoms become more positively charged with a total difference of $+0.24e$, with respect to their charges in SiO_2 without the Ag NP. The charges on the SiO_5 and OSi_3 defects do not change notably whereas the NBO atom becomes more negative by -0.18e and the SiO_3 becomes less positively charged by -0.71e due to its bonding with an Ag atom. By adding all the corresponding charge differences, one finds a total of -3.44e which is not sufficient to counterbalance the loss of 5.05e by the Ag NP. Comparing the total charges on the Si and O atoms in the system with and without the Ag NP without considering the Si* and O* ones, we observe that the O atoms have taken most of the remaining electrons, -1.67e, with respect to -0.87e for the Si ones.

In summary, due to its embedding in an amorphous silica matrix, the Ag_{147} NP (i) forms Si-Ag and O-Ag covalent bonds at the interface which leads to the transfer of $\approx$ -0.8/-0.9e per broken Si-O bond, (ii) looses an additional electronic charge of $\approx$ -2e which is captured by native defects such as NBO or SiO_3 if present and by the oxygen atoms of the matrix on a layer of $\approx$ 5 Å around the nanoparticle. This electron depletion affects mostly the outer shells of the Ag NP which becomes positively charged.

3.3 Concentration and size effects

In order to assess whether these results are dependent on the size of the Ag NP, we have undertaken to simulate an equivalent system but with a Ag NP of 55 atoms, Ag_{55}. The Ag_{55} NP was first

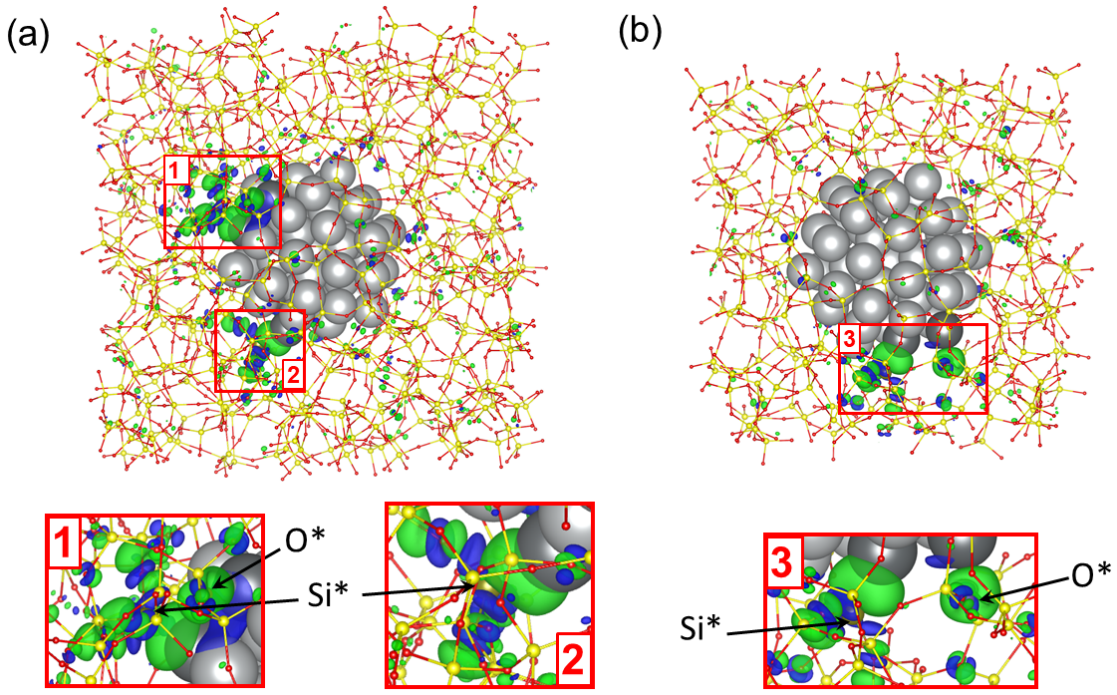

Fig. 6 Isosurfaces of the electron density difference for (a) L-Ag_{55} and (b) S-Ag_{55}. Positive values in green and negative values in blue. Insets show magnification of the interface reconstructions.

introduced in a silica matrix contained in a simulation box of the same size as the Ag_{147} NP system, L = 27.6 Å. In this system, called hereafter L-Ag_{55}, the silica wall is thicker than in the case of L-Ag_{147}. Then, we have modeled an Ag_{55} NP in a smaller periodic box of size L = 22.7 Å, called hereafter S-Ag_{55}, in which the silica walls are of equivalent thickness than in L-Ag_{147}. These systems allow to investigate (i) the effect of the concentration of the NPs by comparing L-Ag_{55} and S-Ag_{55} and (ii) the effect of the size of the Ag NP by comparing L-Ag_{147} and S-Ag_{55}. Note that there are no native defects in the silica matrix in these systems. The evolution of the total energy of these two systems during the successive relaxation steps and the corresponding structures are shown in the Supp. Info (Figure S5).

As for the Ag_{147} system, we observe the breaking of Si-O bonds and the formation of Si-Ag and O-Ag bonds at the interface between the silica and the Ag NP. Two Si-O bonds are broken in L-Ag_{55}, and only one in S-Ag_{55}. Similarly to what happens in L-Ag_{147}, after breaking, the charge goes mainly on the Si^* atoms which carry a charge of $+2.22e$ and $+2.30e$ in the L-Ag_{55} system and $+2.23e$ in the S-Ag_{55} one and the remaining O^*-Si bonds are shorter (around 1.58 Å). In the S-Ag_{55} system, the O^* atom binds to an Ag atom of the Ag NP surface with a bond length of 2.17 Å. In the L-Ag_{55} one, the O^* atoms bridge two Ag atoms of the Ag NP surface with bond lengths of 1.91 Å and 2.02 Å in one case and of 1.85 Å and 2.25 Å in the other case.

Figures 6(a) and (b) show the isosurfaces at 0.003 e/Å^3 isovalue of the electronic density differences for the L-Ag_{55} and S-Ag_{55} systems, respectively. The interface reconstructions are accompanied by significant modifications of the electronic density represented by green and blue isosurfaces for positive and negative values, respectively. However, some smaller isosurfaces can also be distinguished inside the silica matrix away from the interface, as it was the case for the L-Ag_{147} system.

The effect of these reconstructions on the charge distribution inside the Ag_{55} NP can be viewed in Figure 7(a) by comparison to Ag_{55} in vacuum. As for the L-Ag_{147} system, the charges on the Ag NP surface change significantly, especially for the vertex atoms which loose their negative charge. One can also clearly distinguish the Ag atoms which become bonded to Si^* and O^* atoms as their charges become more negative and positive, respectively. These charge modifications are accompanied by important structural changes, in particular at the surface of the Ag NP, as it can be seen in Figure 7(b). As for the L-Ag_{147} NP, mostly the outer shell of the Ag_{55} particle is affected and becomes positively charged except for the Ag atoms bonded to the Si^* atoms.

Finally, as in the L-Ag_{147} system, we have evaluated the total charge on the Ag_{55} NP in the two systems. As in the case of the larger nanoparticles, Ag_{55} loses electrons and carries positive charges of $+2.52e$ in L-Ag_{55} and to $+1.82e$ in S-Ag_{55}. The difference between these two systems comes essentially from the presence of two Si-O bond breakings in the first one and only one in the second case, leading to a total charge of -1.80e and of -0.93e on the involved Si^* atoms, respectively (see Table 2). The corresponding O^* atoms become less negatively charged by a total of $+0.29e$ in the L-Ag_{55} system and by $+0.12e$ in the S-Ag_{55} one, leaving 1.02e and 1.01e electrons unassigned, respectively. Again, we observe that these electrons go preferentially on O atoms inside the matrix, even when they are not bound to Ag atoms of the NP surface. The extension of the charge differences on the O atoms in silica from the surface within the matrix is of $\approx$ 4 Å , i.e.

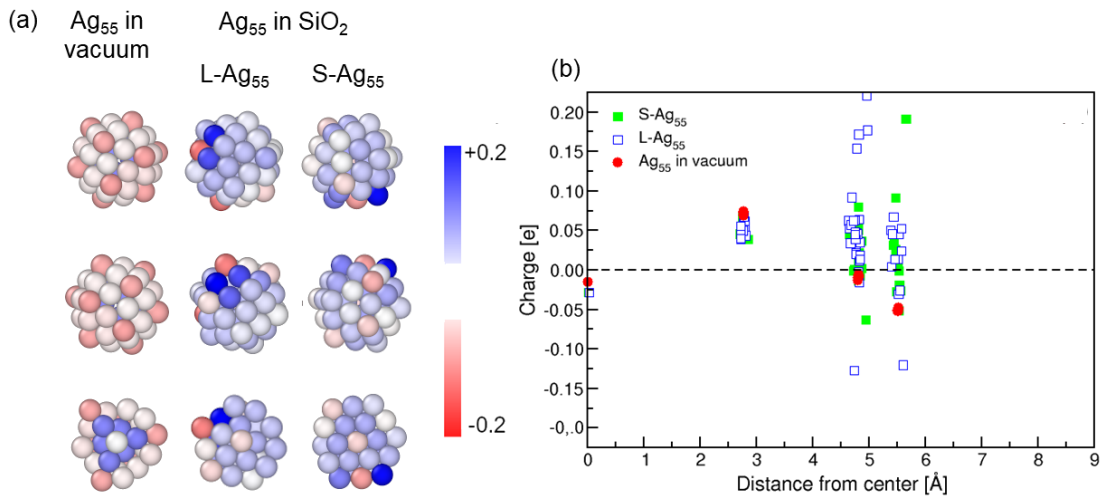

Fig. 7 (a) Charges on the Ag atoms of the Ag_{55} NP in in vacuum (left) and in the SiO_2 matrix (S-Ag_{55}, center and L-Ag_{55}, right).(b) Evolution of the atomic charges on the Ag atoms as a function of their distance to the center of the mass of the NP: Ag_{55} in vacuum (red circles), embedded in SiO_2, L-Ag_{55} (empty blue squares) and S-Ag_{55} (full green squares).

slightly smaller than in the L-Ag_{147} system (see Figure 4(b)).

The comparison of the two systems containing an Ag_{55} NP does not evidence any effect of the interaction of the NP with its periodic images, *i.e.* any concentration effect. This result indicates that a distance of $\approx$ 10 Å between the NPs is sufficient to screen the interactions, which corresponds approximately to 6 SiO_4 tetrahedra in amorphous silica. However, this does not rule out the fact that at higher concentration regimes, the nanoparticles may interact with each other despite the presence of the silica matrix.

As far as size effects are concerned, it is not possible to draw conclusions on their impact on interface reconstructions, given the few statistics available. However, we can note that we do not observe major qualitative differences on the nature of the broken bonds nor on the associated charge transfers. Moreover, these bonds are very similar to those observed in the reconstructions of planar interfaces[39]. The only notable difference between the system with Ag_{147} NP and the system with Ag_{55} NP is the amount of electrons lost by the NP and injected into the silica matrix, in addition to that captured by the broken bonds at the interface. Comparing the L-Ag_{147} system with the L-Ag_{55} system, the charge distributed over the silica matrix is of -1.77e in the first case and -1.01e in the second case. In summary, the number of electrons transferred to the silica matrix in addition to those corresponding to the interface bonds formed does not depend on the concentration of silver nanoparticles inside silica but on the size of the embedded nanoparticles.

4 Conclusion and implications for experiments

Icosahedral Ag NPs of 55 and 147 atoms have been embedded in amorphous silica in cubic boxes with PBCs using Monte Carlo simulations. These configurations have been used as initial positions for atomic positions relaxations by means of dispersion-corrected DFT simulations. In all the investigated systems, we observe the breaking of Si-O bonds close to the Ag NP surface and the formation of Si-Ag bonds and, in some cases, of O-Ag bonds. These latest are observed only when the broken Si-O bond belongs to a large ($>$ 5-membered) ring perpendicular to the Ag NP surface. These interface reconstructions are accompanied by an electron depletion of the Ag NP and an associated important redistribution of the charges inside the Ag NP and the matrix.

By comparison with our previous study on planar Ag/SiO_2 interfaces[39], the number of created bonds at the interface is much lower (around 0.30 bonds/nm^2 for Ag_{55} and 0.45 bonds/nm^2 for Ag_{147} with respect to 1.5 to 2.2 bonds/nm^2 for the planar interfaces[39]). This can be explained by the fact that the Ag(111) and Ag(110) surfaces are quite small in these Ag NPs and that the interface is not planar but curved. Some distances between the Si and O atoms of silica and the Ag atoms of the NP surface may be too large to initiate the interface bond formation. The curvature of the interface may also play a role in the fact that some of the O* atoms do not link to a surface Ag atom but prefer to move away from the NP, due to high internal strain. From a quantitative point of view, a large part of the charge lost by the Ag NP is due to the Si-Ag bonds formed at the interface, since roughly 0.9e is donated per each of them. However, this does not account for the total amount of charge lost and the remainder of the electrons lost can be estimated around 1.8e for Ag_{147} and 1.0e for Ag_{55} if the particle is embedded in a defect-free silica. Interestingly, the ratio between the remainder charge lost by the Ag_{147} and that lost by the Ag_{55} (1.8) is very close to the ratio between their surface area ($\approx$1.75 in vacuum using the formula from[56]), rather than to the ratio between their number of atoms (2.67) nor between their volume (2.35). This would imply that the electrostatic charging of silica around the Ag NP depends on the interface area. Nevertheless, this proportionality between the number of electrons captured by the matrix and the surface of the Ag NP must be confirmed on a larger number of Ag NP sizes. In addition, the extent of the electronic displacement is about 1 to 2 layers inside the Ag NP and a few angströms inside the matrix where the captured

electrons are mostly found on the more electronegative oxygen species. This extension of the electron density in the matrix goes far beyond the extension of the Ag NP spill-out since the latter is estimated to be of 1 to 2 Å[23].

When native defects are present in silica, they contribute to the electron depletion from the Ag NP, even if they are located far away from the NP (*i.e.* at distances larger than 4-5 Å), provided that they are electron acceptors such as NBO and SiO_3. The concentration of these defects in our model (around $10^{20}cm^{-3}$) is much higher than in irradiated silica (around $10^{18}cm^{-3}$) however their contribution to the electron depletion from the Ag NP may not be negligible. The presence of electrons trapped on defects in the matrix which is predicted by our simulations will impact the conduction properties of the nanocomposite layer and could likely explain previous experimental results. Recently the optical transfer of charge carriers has been demonstrated between a single plane of Ag NPs and a graphene flake deposited on top of a nanometer sized silica cover layer[57] by simply analyzing the Raman scattering signal of the 2D layer. Hence, a selective activation of D Raman modes has been observed in the entire graphene sheet and has been ascribed to the change of electron–phonon interactions and quantum pathways in the few layers graphene due to the presence of injected carriers. This charge injection is confirmed by the rather strong background in the Raman signal of the graphene sheet, due to electronic Raman scattering. Free carrier lifetime as short as 50 fs has been measured and this shortness has been ascribed to defects in the silica top layer or at the interface/graphene due to the synthesis process. We can infer that the trapped electrons in the silica matrix at the neighborhood of the Ag NPs predicted by our simulations could trigger the easy electronic transfer to the top graphene layer under light excitation. In a different study[58], electron transport devices have been designed that electrically address an embedded assembly of Ag NPs for current-voltage I-V characterization. While the reference sample without Ag NPs shows a resistance of tens of TΩ, the one with Ag NPs exhibits a ten times lower resistance. In addition, several down-switching sharp peaks appearing in the forward sweeps brought to the conclusion that tunneling current does not pass uniformly through the whole NPs assembly, but through narrow leakage paths within the oxide[58]. This observation is again compatible with the presence of trapped electrons in the oxide matrix, as predicted in the present work.

The Ag NP chemical, electrochemical and optical properties can also be expected to be modified as the particle becomes positively charged. In particular, the fact that the surface atoms are predominantly positive will inevitably have an impact on its surface reactivity. However, without further investigation, it is difficult to speculate on the actual effects and on which type of reactions this may have the most significant impact. In any case, the Ag NP dissolution mechanisms and consequently the Ag^+ release could be affected. Concerning optical properties, an evaluation of the potential LSPR shift due to a change in the number of conduction electrons is currently in progress in our group and will be the subject of a forthcoming paper. In particular, central questions are whether the LSPR shift would be significant enough to be experimentally detectable and consistent with experimental observations[23].

Conflicts of interest

There are no conflicts to declare.

Acknowledgements

The authors thank Arnaud Arbouet, Robert Carles, Matthias Hillenkamp, Jean Lermé, Clément Majorel and Hans-Christian Weissker for very helpful discussions. This work was supported by the ANR grant "BENDIS" (ANR-21-CE09-0008) and was granted access to the HPC resources of supercomputing centers (CALMIP under the allocation p17024 and GENCI under the allocation A0080910409).

Notes and references

1 M. Skonieczna and D. Hudy, *Silver Nanoparticles*, IntechOpen, Rijeka, 2018, ch. 7.

2 D. D. Evanoff Jr. and G. Chumanov, *ChemPhysChem*, 2005, **6**, 1221–1231.

3 C. Caro, P. M. Castillo, R. Klippstein, D. Pozo and A. P. Zaderenko, *Silver Nanoparticles*, IntechOpen, Rijeka, 2010, ch. 11.

4 M. Sabela, S. Balme, M. Bechelany, J.-M. Janot and K. Bisetty, *Advanced Engineering Materials*, 2017, **19**, 1700270.

5 Y. Hu, Y. Shi, H. Jiang, G. Huang and C. Li, *ACS Applied Materials & Interfaces*, 2013, **5**, 10643–10649.

6 H. Wei, in *Plasmonic Silver Nanoparticles for Energy and Optoelectronic Applications*, John Wiley Sons, Ltd, 2011, pp. 171–184.

7 L. P. Silva, A. P. Silveira, C. C. Bonatto, I. G. Reis and P. V. Milreu, *Nanostructures for Antimicrobial Therapy*, Elsevier, 2017, pp. 577 – 596.

8 P. Prasher, M. Singh and H. Mudila, *3 Biotech*, 2018, **8**, 411.

9 K. Zheng, M. I. Setyawati, D. T. Leong and J. Xie, *Coordination Chemistry Reviews*, 2018, **357**, 1 – 17.

10 T. Zhang, L. Wang, Q. Chen and C. Chen, *Yonsei Medical Journal*, 2014, **55**, 283.

11 Z. Ferdous and A. Nemmar, *International journal of molecular sciences*, 2020, **21**, 2375.

12 A. Matikainen, T. Nuutinen, T. Itkonen, S. Heinilehto, J. Puustinen, J. Hiltunen, J. Lappalainen, P. Karioja and P. Vahimaa, *Scientific Reports*, 2016, **6**, 37192.

13 B. T. Reagor and J. D. Sinclair, *Journal of The Electrochemical Society*, 1981, **128**, 701–705.

14 C. Levard, E. M. Hotze, B. P. Colman, A. L. Dale, L. Truong, X. Y. Yang, A. J. Bone, G. E. Brown, R. L. Tanguay, R. T. Di Giulio, E. S. Bernhardt, J. N. Meyer, M. R. Wiesner and G. V. Lowry, *Environmental Science & Technology*, 2013, **47**, 13440–13448.

15 H. M. Fahmy, A. M. Mosleh, A. A. Elghany, E. Shams-Eldin, E. S. Abu Serea, S. A. Ali and A. E. Shalan, *RSC Advances*, 2019, **9**, 20118–20136.

16 N. Alissawi, T. Peter, T. Strunskus, C. Ebbert, G. Grundmeier and F. Faupel, *Journal of Nanoparticle Research*, 2013, **15**, 2080.

17 I. Ali, M. R. Akl, G. A. Meligi and T. A. Saleh, *Results in Physics*, 2017, **7**, 1319 – 1328.

18 B. Pant, M. Park and S. Park, *Polymers (Basel).*, 2019, **11**, 1185.

19 C. Liao, Y. Li and S. Tjong, *Int J Mol Sci.*, 2019, **20**, 449.

20 G. Walters and I. P. Parkin, *J. Mater. Chem.*, 2009, **19**, 574–590.

21 K. M. Mayer and J. H. Hafner, *Chemical Reviews*, 2011, **111**, 3828–3857.

22 M. Zapata Herrera, J. Aizpurua, A. K. Kazansky and A. G. Borisov, *Langmuir*, 2016, **32**, 2829–2840.

23 A. Campos, N. Troc, E. Cottancin, M. Pellarin, H.-C. Weissker, J. Lermé, M. Kociak and M. Hillenkamp, *Nat. Phys.*, 2019, **15**, 275–280.

24 Y. Kobayashi, H. Katakami, E. Mine, D. Nagao, M. Konno and L. M. Liz-Marzán, *Journal of Colloid and Interface Science*, 2005, **283**, 392 – 396.

25 N. M. Bahadur, T. Furusawa, M. Sato, F. Kurayama, I. A. Siddiquey and N. Suzuki, *Journal of Colloid and Interface Science*, 2011, **355**, 312 – 320.

26 X. Liu, D. Li, X. Sun, Z. Li, H. Song, H. Jiang and Y. Chen, *Scientific Reports*, 2015, **5**, 12555.

27 C. R. Yonzon, D. A. Stuart, X. Zhang, A. D. McFarland, C. L. Haynes and R. P. Van Duyne, *Talanta*, 2005, **67**, 438 – 448.

28 J. N. Anker, W. P. Hall, O. Lyandres, N. C. Shah, J. Zhao and R. P. Van Duyne, *Nature Materials*, 2008, **7**, 442.

29 G. A. Sotiriou, T. Sannomiya, A. Teleki, F. Krumeich, J. Vörös and S. E. Pratsinis, *Advanced Functional Materials*, 2010, **20**, 4250–4257.

30 S. Mitra, R. Chattopadhyay, M. Pal, G. P. Das and S. K. Bhadra, *Physica E: Low-dimensional Systems and Nanostructures*, 2019, **112**, 26–35.

31 H. Hofmeister, G. Tan and M. Dubiel, *Journal of Materials Research*, 2005, **20**, 1551–1562.

32 A. C. Ngandjong, C. Mottet and J. Puibasset, *The Journal of Physical Chemistry C*, 2016, **120**, 8323–8332.

33 M. Hillenkamp, G. D. Domenicantonio, O. Eugster and C. Félix, *Nanotechnology*, 2007, **18**, 015702.

34 P. Benzo, L. Cattaneo, C. Farcau, A. Andreozzi, M. Perego, G. Benassayag, B. Pécassou, R. Carles and C. Bonafos, *Journal of Applied Physics*, 2011, **109**, 103524.

35 Z. She, R. Li, W. Guo, H. Xue and X. Zhang, *Journal of Asian Ceramic Societies*, 2020, **8**, 597–604.

36 A. M. Shor, S. S. Laletina, E. A. Ivanova Shor, V. A. Nasluzov, V. I. Bukhtiyarov and N. Rösch, *Surface Science*, 2014, **630**, 265–272.

37 S. Ramalingam, L. B. Devi, J. Raghava Rao and B. Unni Nair, *RSC Adv.*, 2014, **4**, 56041–56051.

38 J. Peszke, M. Dulski, A. Nowak, K. Balin, M. Zubko, S. Sułowicz, B. Nowak, Z. Piotrowska-Seget, E. Talik, M. Wojtyniak, A. Mrozek-Wilczkiewicz, K. Malarz and J. Szade, *RSC Adv.*, 2017, **7**, 28092–28104.

39 H. Balout, N. Tarrat, J. Puibasset, S. Ispas, C. Bonafos and M. Benoit, *ACS Applied Nano Materials*, 2019, **2**, 5179–5189.

40 P. Gangopadhyay, R. Kesavamoorthy, K. G. M. Nair and R. Dhandapani, *Journal of Applied Physics*, 2000, **88**, 4975–4979.

41 B. Sun and A. S. Barnard, *Nanoscale*, 2017, **9**, 12698–12708.

42 B. Sun, M. Fernandez and A. S. Barnard, *Journal of Chemical Information and Modeling*, 2017, **57**, 2413–2423.

43 Q. Fu and T. Wagner, *Surface Science Reports*, 2007, **62**, 431–498.

44 M. Komiyama and T. Shimaguchi, *Surface and Interface Analysis*, 2001, **32**, 189–192.

45 A. M. Eremenko, N. P. Smirnoval, I. P. Mukhal and H. R. Yashan, *Theoretical and Experimental Chemistry*, 2010, **46**, 65–88.

46 R. Ferullo, G. Garda, P. Belelli, M. Branda and N. Castellani, *Journal of Molecular Structure: THEOCHEM*, 2006, **769**, 217–223.

47 J. Lermé, B. Palpant, B. Prével, M. Pellarin, M. Treilleux, J. L. Vialle, A. Perez and M. Broyer, *Phys. Rev. Lett.*, 1998, **80**, 5105–5108.

48 L. Papa, I. C. de Freitas, R. S. Geonmonond, C. B. de Aquino, J. C. Pieretti, S. H. Domingues, R. A. Ando and P. H. C. Camargo, *J. Mater. Chem. A*, 2017, **5**, 11720–11729.

49 S. Tsuneyuki, M. Tsukada, H. Aoki and Y. Matsui, *Physical Review Letters*, 1988, **61**, 869–872.

50 Y. Guissani and B. Guillot, *The Journal of Chemical Physics*, 1996, **104**, 7633–7644.

51 A. C. Ngandjong, C. Mottet and J. Puibasset, *The Journal of Physical Chemistry C*, 2017, **121**, 3615–3622.

52 J. P. Perdew and W. Yue, *Phys. Rev. B*, 1986, **33**, 8800–8802.

53 S. Grimme, J. Antony, S. Ehrlich and H. Krieg, *The Journal of Chemical Physics*, 2010, **132**, 154104.

54 J. P. Allen, D. O. Scanlon and G. W. Watson, *Physical Review B*, 2011, **84**, 115141.

55 J. Zhou, Z.-H. Li, W.-N. Wang and K.-N. Fan, *Chemical Physics Letters*, 2006, **421**, 448–452.

56 B. Molleman and T. Hiemstra, *Physical Chemistry Chemical Physics*, 2018, **20**, 20575–20587.

57 R. Carles, M. Bayle and C. Bonafos, *Nanotechnology*, 2018, **29**, 175301.

58 M. Bayle, J. Grisolia, G. Ben Assayag, B. Pecassou, C. Bonafos, P. Benzo, F. Gourbilleau and R. Carles, *physica status solidi c*, 2015, **12**, 1328–1332.